Letter

Synthetic Landau levels and robust chiral edge states for dark-state polaritons in a static and scalable continuum media

Yu-Hung Kuan,[1] Shin-Yu Lee,[1] Siang-Wei Shao,[1] Wu-Cheng Chiang,[1] I-Kang Liu,[2] Julius Ruseckas,[3,4] Gediminas Juzeliūnas,[4] Yu-Ju Lin,[5,6,*] and Wen-Te Liao[1,7,8,†]

[1]*Department of Physics, National Central University, Taoyuan City 32001, Taiwan*
[2]*Joint Quantum Centre Durham-Newcastle, School of Mathematics, Statistics and Physics, Newcastle University, Newcastle upon Tyne, NE1 7RU, United Kingdom*
[3]*Baltic Institute of Advanced Technology, Pilies gatvė 16-8, LT-01403 Vilnius, Lithuania*
[4]*Institute of Theoretical Physics and Astronomy, Vilnius University, Saulėtekio 3, LT-10257 Vilnius, Lithuania*
[5]*Institute of Atomic and Molecular Sciences, Academia Sinica, Taipei 10617, Taiwan*
[6]*Department of Physics, National Tsing Hua University, Hsinchu 30013, Taiwan*
[7]*Physics Division, National Center for Theoretical Sciences, Taipei 10617, Taiwan*
[8]*Quantum Technology Center, National Central University, Taoyuan City 32001, Taiwan*

(Received 30 December 2022; revised 10 July 2023; accepted 19 October 2023; published 27 November 2023)

We demonstrate the generation and dynamical control of synthetic Landau levels and robust chiral edge states for neutral dark-state polaritons using electromagnetically induced transparency in our theoretical studies. We adopt an optical approach to produce synthetic magnetic fields for dark-state polaritons in the static laboratory frame. In our scalable system, an Aharonov-Bohm phase is obtained along a closed loop in a continuous material rather than a sophisticated lattice structure. Our scheme paves the way toward versatile quantum simulators, dynamically controllable photonic circuits, and generators for exotic states of light carrying topological winding numbers.

DOI: 10.1103/PhysRevResearch.5.L042029

The discovery of the quantum Hall effects [1–6] inspired the remarkable progress in emulating the synthetic gauge fields for electrically neutral particles which do not experience the Lorentz force. Successful implementations include ultracold atoms [7–13], photons [14–27], and electronic circuits [28]. Most pioneering works in photonics use sophisticated periodic structures of resonators [14–19,21–24,27,29] or an elaborated optical trajectory [20,26] to produce synthetic gauge fields and robust chiral edge states for photons [25]. Among photonic systems, electromagnetically induced transparency (EIT) [30–35] has attracted extensive studies on slow [36–40] and stationary [41–44] light in continuum media. EIT leads to electrically neutral quasiparticles known as dark-state polaritons (DSPs) [38,39,42,43]. DSPs can interact strongly via atom-atom interaction [26,45–52] and should facilitate creation of strongly correlated DSP quantum states under synthetic gauge fields, e.g., the fractional quantum Hall states [26,53]. Yet, up to now, only mechanical rotation [54] is considered for creating the synthetic gauge fields for DSPs in the rotating frame. Here, we demonstrate an optical method to generate Landau levels (LLs) and robust chiral edge states for the atomic coherence of the DSPs in a lattice-free medium. Our scheme generates synthetic gauge fields in the static laboratory frame and thus avoids problems associated with mechanical rotations [54], such as excitations [55] and destabilization [56]. Moreover, our lattice-free system is scalable; namely, one can scale up the size of the synthetic quantum states and study the gauge fields in the expanded system. This makes a building block for more complex systems, such as bosonic quantum Hall states. The lattice-free platform also allows for easier access to interactions with Rydberg EIT. Yet, unlike static photonic structures, our system is dynamically controllable and can lead to fast control over photonic flow like a circuit. Furthermore, the present EIT-based system can potentially simulate a charged particle in a magnetic field [26,53,54], nonlinear optics [57], negative-mass dynamics [58], and non-Hermitian quantum mechanics [59,60].

Figure 1 depicts our system. A two-dimensional atomic medium is coupled to four control (probe) fields propagating along four directions indicated by thick red (blue) arrows. Figure 1(a) illustrates the typical stationary-light setup where counterpropagating control fields are aligned [41–44]. We consider the three-level Λ-type system in Fig. 1(b), and each control (probe) field drives a $|2\rangle \rightarrow |3\rangle$ ($|1\rangle \rightarrow |3\rangle$) transition with Rabi frequency $\Omega^{j}_{c(p)}$, where index $j = F, B, R$, and L indicates the forward, backward, rightward, and leftward quantity, respectively. The imaging beam (green thick arrow) in Figs. 1(a) and 1(b) drives the $|2\rangle \rightarrow |4\rangle$ transition and yields the absorption imaging of DSPs [61]. $\Delta_{c(p)}$ is the one-photon

*linyj@gate.sinica.edu.tw
†wente.liao@g.ncu.edu.tw

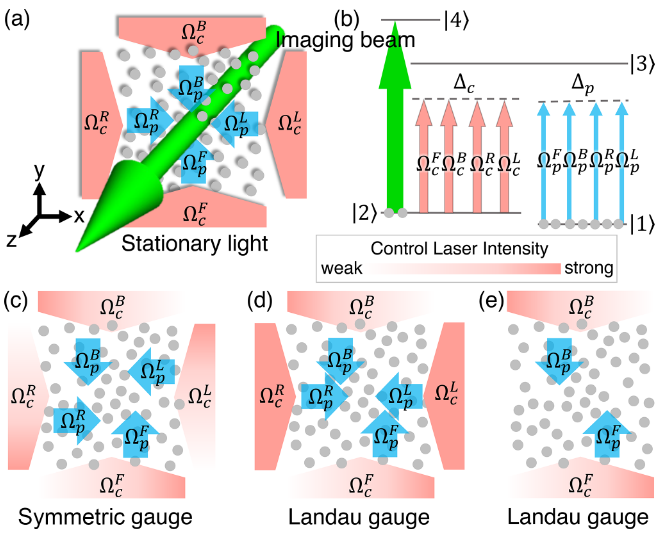

FIG. 1. (a) Two-dimensional EIT-stationary-light system. Gray dots illustrate atoms, and red (blue) thick arrows depict control (probe) fields. (b) Red (blue) upward-pointing arrows represent the control (probe) fields driving transition $|2\rangle \to |3\rangle$ ($|1\rangle \to |3\rangle$) with detuning $\Delta_{c(p)}$. The color gradient of each red arrow illustrates the transverse intensity of a control laser. An aligned $\Omega_p^F - \Omega_p^B$ or $\Omega_p^R - \Omega_p^L$ blue arrow pair represents stationary light, and a misaligned blue arrow indicates the slow light. Green thick arrows [along z in (a), and upward in (b)] depict the imaging beam which drives transition $|2\rangle \to |4\rangle$ for the visualization of DSPs. (c)–(e) Generation of the synthetic vector potential of the symmetric gauge (c) and Landau gauge [(d) and (e)].

detuning of the control (probe) fields. Our system is described by optical-Bloch equations [38,41,44,62,63]

$$\frac{\partial \rho_{21}}{\partial t} = i(\Delta_c - \Delta_p)\rho_{21} + \frac{i}{2}\sum_j \Omega_c^{j*}\rho_{31}^j, \quad (1)$$

$$\frac{\partial \rho_{31}^j}{\partial t} = \frac{i}{2}\Omega_p^j + \frac{i}{2}\Omega_c^j\rho_{21} - \left(\frac{\Gamma}{2} + i\Delta_p\right)\rho_{31}^j, \quad (2)$$

$$\frac{1}{c}\frac{\partial \Omega_p^j}{\partial t} + \epsilon_j\frac{\partial \Omega_p^j}{\partial X_j} = i\eta\rho_{31}^j, \quad (3)$$

where ρ_{21} (ρ_{31}^j) is the coherence between state $|2\rangle$ ($|3\rangle$) and $|1\rangle$. ρ_{31}^j quantifies the polarization and the dispersion relation to Ω_p^j. Γ is the spontaneous decay rate of state $|3\rangle$. $\eta = \frac{\Gamma\xi_x}{2L_x} = \frac{\Gamma\xi_y}{2L_y}$ is the light-matter coupling constant. ξ_x (ξ_y) and L_x (L_y) are the optical depth and the medium length in the x (y) direction, respectively. $\epsilon_{F(R)} = 1$, $\epsilon_{B(L)} = -1$, $X_{R(L)} = x$, and $X_{F(B)} = y$ indicate the Ω_p^j propagating direction. The ground-state coherence ρ_{21} dominates the DSP, and we derive its governing equation in the following steps. Neglecting $\frac{1}{c}\frac{\partial \Omega_p^j}{\partial t}$ in Eq. (3) as typically adopted in EIT [38], multiplying both sides of Eq. (3) by Ω_c^{j*}, and then summing Eq. (3) over j lead to $\sum_j \epsilon_j \Omega_c^{j*}\frac{\partial \Omega_p^j}{\partial X_j} = i\eta\sum_j \Omega_c^{j*}\rho_{31}^j$. By replacing the right-hand side of the above relation with Eq. (1), and substituting the adiabatic condition [38] $\Omega_p^j = -[1 + \epsilon_j(\frac{2\Delta_p - i\Gamma}{i\eta})\frac{\partial}{\partial X_j}]\Omega_c^j\rho_{21}$ on its left-hand side, we obtain a Schrödinger-like equation

$$i\hbar\frac{\partial \rho_{21}}{\partial t} = \frac{\left(\frac{\hbar}{i}\nabla + \vec{A}\right)^2}{2m}\rho_{21} + U\rho_{21} + i\left(\frac{\Gamma}{2\Delta_p}\right)\frac{\hbar^2}{2m}\nabla^2\rho_{21} \quad (4)$$

when $\frac{\partial \Omega_c^j}{\partial X_j}$ and $\frac{\partial^2 \Omega_c^j}{\partial X_j^2}$ are negligible. Here, ρ_{21} plays the role of wave function, the synthetic vector potential $\vec{A} = m\vec{V}_g$ for charge $q = -1$, the scalar potential $U = \hbar(\Delta_p - \Delta_c) - \frac{m}{2}|\vec{V}_g|^2$, and $\hbar$ is the reduced Planck constant. $\vec{V}_g = (V_R - V_L, V_F - V_B) = \frac{1}{2\eta}(|\Omega_c^R|^2 - |\Omega_c^L|^2, |\Omega_c^F|^2 - |\Omega_c^B|^2)$ is the EIT propagation velocity [44]. We use constant Δ_p, η, Ω_c, and $V_R + V_L = V_F + V_B = \frac{\Omega_c^2}{2\eta}$ to get the uniform effective mass $m = \frac{\hbar\eta^2}{2\Delta_p\Omega_c^2}$. Equation (4) suggests that our scheme can create versatile quantum simulators by optically engineering the Hamiltonian. Furthermore, the $\vec{A}^2$ and Δ_p-dependent m can potentially simulate nonlinear optics [57] and negative-mass dynamics [58]. The last diffusion term allows for the study of non-Hermitian quantum mechanics [59,60]. We emphasize that the design of our system is guided by Eq. (4), and all of the following results are given by full numerical calculations of Eqs. (1)–(3).

We first demonstrate three possible schemes to produce LLs [4–6,20,25,64,65] for DSPs. One can engineer different gauges for $\vec{A}$, e.g., by choosing our first scheme with $\Omega_c^R = \frac{\Omega_c}{2}\sqrt{1 - \frac{y}{L_y}}$, $\Omega_c^L = \frac{\Omega_c}{2}\sqrt{1 + \frac{y}{L_y}}$, $\Omega_c^F = \frac{\Omega_c}{2}\sqrt{1 + \frac{x}{L_x}}$, $\Omega_c^B = \frac{\Omega_c}{2}\sqrt{1 - \frac{x}{L_x}}$, and $L_x = L_y = L$, which leads to the symmetric-gauge $\vec{A} = \frac{\hbar\eta}{8L\Delta_p}(-y, x)$ as depicted in Fig. 1(c). Given that the control laser intensity is proportional to $|\Omega_c^j|^2$, our $\vec{A}$ can be realized by using four control lasers with gradients of transverse intensity; e.g., the forward one is proportional to $1 + \frac{x}{L_x}$ as illustrated in Fig. 1(c). The transverse intensity profile remains unchanged along the beam propagating direction within Rayleigh range > 1 m, given by beam size $\approx L_x, L_y > 1$ mm in our system and optical wavelength $\lesssim 1$ μm. Thus the control beams remain collimated within the atomic cloud. For simplicity, we utilize the Landau-gauge $\vec{A} = \frac{\hbar\eta}{4L_x\Delta_p}(0, x)$ using the second design with $\Omega_c^R = \Omega_c^L = \frac{\Omega_c}{\sqrt{2}}$, $\Omega_c^F = \frac{\Omega_c}{\sqrt{2}}\sqrt{1 + \frac{x}{L_x}}$, and $\Omega_c^B = \frac{\Omega_c}{\sqrt{2}}\sqrt{1 - \frac{x}{L_x}}$ as illustrated in Fig. 1(d). We also use $\Delta_c = \Delta_p - \frac{\Omega_c^2}{16\Delta_p L_x^2}x^2$ to make $U = 0$, which can be implemented by position-dependent Zeeman or Stark shifts of atomic levels [54,66,67]. These lead to LLs in the Landau gauge, $\rho_{21}^{(n)}(x, y, t) = H_n(\frac{x + kl_B^2}{l_B})\exp\{-(\frac{x + kl_B^2}{\sqrt{2}l_B})^2 + i[ky - (n + \frac{1}{2})\omega_B t]\}$, where H_n is the Hermite polynomial. The cyclotron frequency $\omega_B = \Omega_c^2/(\xi_x\Gamma)$, and the magnetic length $l_B = \sqrt{\hbar/m\omega_B} = L_x\sqrt{8\Delta_p/(\xi_x\Gamma)}$. Moreover, the third scheme, depicted in Fig. 1(e), utilizes only two control beams $\Omega_c^F = \frac{\Omega_c}{\sqrt{2}}\sqrt{1 + \frac{x}{L_x}}$ and $\Omega_c^B = \frac{\Omega_c}{\sqrt{2}}\sqrt{1 - \frac{x}{L_x}}$. Here one can introduce the transverse effective mass $m_\perp = \frac{2\eta\hbar k_p}{\Omega_c^2}$ differing from the longitudinal m, where k_p is the angular wave number of the probe field [54]. The above three schemes result in a uniform synthetic magnetic field $\vec{B} = \frac{\hbar\eta}{4L_x\Delta_p}\hat{e}_z$.

Noting that the optical depth is a key parameter in EIT physics [68–70], we envisage using $\xi_{x(y)} \leqslant 2000$ for atoms trapped in a pancake geometry with size $L_{x(y)} \sim$ millimeters.

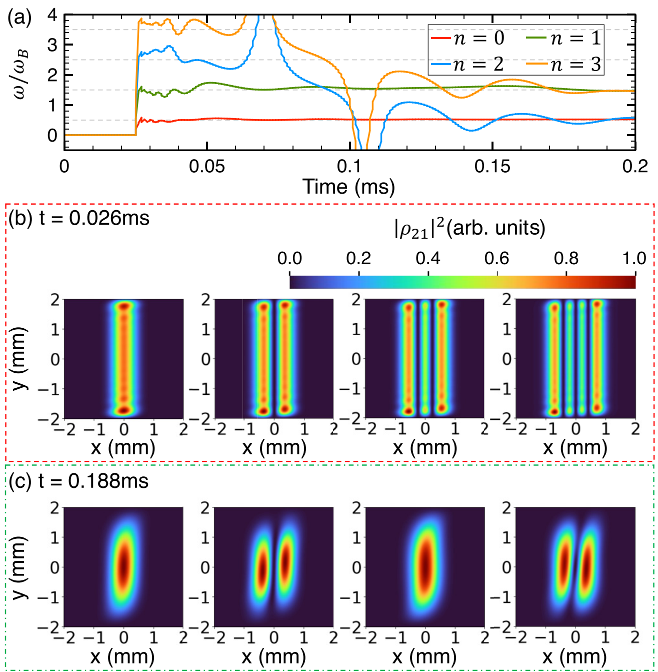

FIG. 2. (a) Time evolution of the angular frequency of the DSP in the nth LL. Solid red, green, blue, and orange curves depict $n = 0$, 1, 2, and 3, respectively. (b) and (c) The spatial profile of the nth LL at $t = 0.026$ ms, when the Landau-gauge environment is switched on (b), and at $t = 0.188$ ms (c). The maximum $|\rho_{21}|^2$ is normalized to 1.

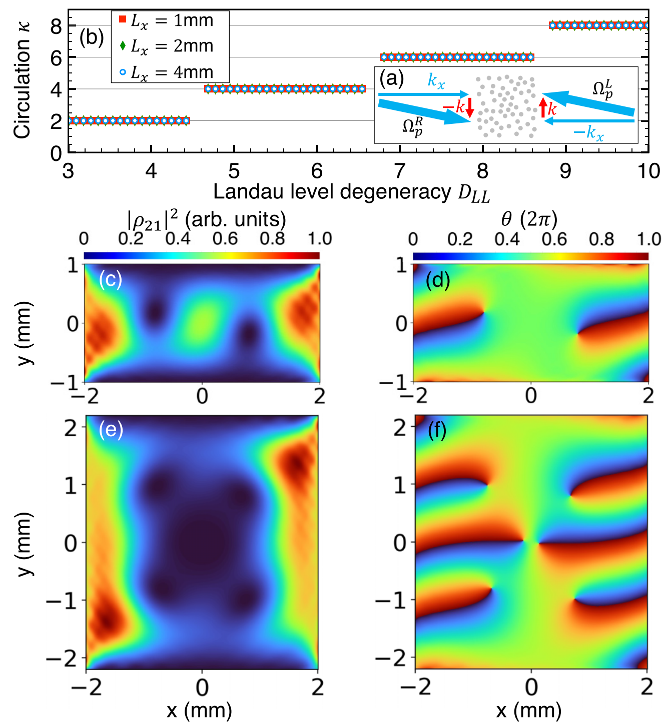

FIG. 3. Steady state ρ_{21} under suitable boundary conditions in (a) with slightly tilted probe beams. (b) D_{LL}-dependent circulation quanta κ for $L_x = 1$ mm (red squares), 2 mm (green diamonds), and 4 mm (blue circles) for $(l_B/L_x, \xi_x) = (0.15, 2000)$. (c) $|\rho_{21}|^2$ and (d) phase θ for $L_y = 2$ mm and $D_{\mathrm{LL}} = 3.5$. (e) $|\rho_{21}|^2$ and (f) θ for $L_y = 4.4$ mm and $D_{\mathrm{LL}} = 7.8$.

The size can be made larger under suitable design of the optical setup. To have a spatially uniform $\eta \propto n_{3\mathrm{D}}$, one can implement a uniform three-dimensional (3D) particle density $n_{3\mathrm{D}}$ using a box potential [71,72] for the x and y confinement by the optical relay. The millimeter-size trap is achievable by using large aperture optics along with sufficient optical power. Indeed, optical depth over 1300 has been realized in nonuniform clouds [68–70]. One can start with a nonuniform 3D cloud with $n_{3\mathrm{D}} = 2.7 \times 10^{11}$ cm^{-3} and 1.3×10^{10} atoms [68] and perform forced-evaporative cooling to increase $n_{3\mathrm{D}}$ to 2.7×10^{12} cm^{-3}. We estimate that with such $n_{3\mathrm{D}}$ one can reach $\xi_{x(y)} = 2000$ with $L_{x(y)} = 2$ mm and $L_z \approx 0.2$ mm [73]. Moreover, DSPs' dynamics can be probed by directly measuring $\rho_{22}(x, y, t) \approx |\rho_{21}(x, y, t)|^2$ via the imaging beam in Fig. 1 [61], or by detecting $\rho_{21}(x, y, t)$ via density matrix reconstruction [74] or the EIT retrieval [34,70,75–77] at different directions as is done in tomography. We prepare the nth LL $\rho_{21}^{(n)}(x, y, t = 0)$ with $k = 0$ and observe its evolution. The dynamics of $\rho_{21}^{(n)}$ in the presence of $\vec{A}$ shows two features: (i) Its eigen angular frequency $\omega = (n + 1/2)\omega_B$, and (ii) the last diffusion term in Eq. (4) causes the decay from $\rho_{21}^{(n+2)}$ to $\rho_{21}^{(n)}$, as illustrated in Fig. 2. $\rho_{21}^{(n)}$ is initially prepared by the EIT light storage for $t < 0.025$ ms [34]. Subsequently, we switch on the Landau-gauge EIT environment at $t = 0.025$ ms and analyze its evolution. In Fig. 2(a), gray dashed lines depict the theoretical $\omega_n/\omega_B = (n + 1/2)$. We calculate the angular frequency of ρ_{21} via $\omega = i(\partial_t\rho_{21})/\rho_{21}$ and illustrate them with solid curves for $n = 0, 1, 2, 3$, with the following parameters: $\Gamma = 2\pi \times 5.2$ MHz, $\Delta_p = 1.26\Gamma$, $\Omega_c = 1.84\Gamma$, $\xi_x = \xi_y = 1400$, and $L_x = L_y = 4$ mm, which result in $\omega_B = 2.4 \times 10^{-3}\Gamma$, and $l_B = 0.34$ mm. During 0.025 ms $< t <$ 0.08 ms there are four branches of the numerically solved ω matching the theoretical values very well up to 0.06 ms. Later on, the four branches converge in only two bands, which manifests prediction (ii). Figure 2(b) demonstrates the snapshot of $|\rho_{21}|^2$ for different input n at $t = 0.026$ ms, and Fig. 2(c) shows the results at $t = 0.188$ ms. One can observe that only $\Delta n = 2$ transitions occur. We then investigate the DSP characteristics with suitable injection of probe fields. We initially turn on all control fields to generate an in-plane synthetic $\vec{B}$ and then pump the system by probe fields with Landau level boundary conditions $\Omega_p^R(-L_x/2, y) = \exp(-i\omega_B t - iky)$ and $\Omega_p^L(L_x/2, y) = \exp(-i\omega_B t + iky)$ with $k = L_x/(2l_B^2)$. This can be implemented by using two slightly tilted probe fields with wave vectors $(\mp k_x, \pm k)$ in Fig. 3(a), where $k_x \approx k_p$. The $\exp(-i\omega_B t)$ term can be realized by a phase modulation. The pumping frequency ω_B is chosen in the gap between $n = 0$ and $n = 1$ LL such that no eigenstate is excited in the bulk region. We analyze the steady-state $\rho_{21}(x, y) = |\rho_{21}(x, y)|e^{i\theta(x,y)}$ [78] by calculating the circulation $\kappa = \frac{1}{2\pi}\oint \vec{V}_p \cdot d\vec{l}$ along the system edge as a function of LL degeneracy $D_{\mathrm{LL}} = L_x L_y/(2\pi l_B^2)$, where the current $\vec{V}_p = \nabla\theta$. With $(\xi_x, l_B/L_x, \omega_B, \Omega_c, \Delta_p) = (2000, 0.15, 1.7 \times 10^{-3}\Gamma, 1.84\Gamma, 5.62\Gamma)$, we sweep D_{LL} via elongating L_y and fixing $L_x = 1$, 2, and 4 mm, respectively. Figure 3(b) depicts the quantization of κ for a fixed $l_B/L_x = 0.15$, i.e., the relative size of $n = 1$ LL wave function to the medium length. Remarkably, our scalable system reveals a general feature that the κ plateaus are identical for different L_x. Each plateau indicates an equal number of vortices forming under $\vec{A}$. Using $(L_x, L_y) = (4\text{ mm}, 2\text{ mm})$, where $D_{\text{LL}} = 3.5$, we demonstrate $|\rho_{21}|^2$ and the phase θ in Figs. 3(c) and 3(d), respectively. Figure 3(c) illustrates an array of two vortices whose cores are located in each hollow of $|\rho_{21}|^2$. Figure 3(d) indicates that the topological winding number is 1 for each loop enclosing a vortex core. We numerically calculate the circulation $\kappa = \frac{1}{2\pi}\iint(\nabla \times \vec{V}_p)\cdot \hat{z}dxdy = 2$, which coincides with the number of vortices. Next, we increase D_{LL} to 7.8 by increasing L_y to 4.4 mm in Figs. 3(e) and 3(f). The phase in Fig. 3(f) manifests that the total vortex number and κ become 6. Notably, Fig. 3(e) shows the emergence of a DSP edge state and suggests a transition from a vortex array to an edge flow upon increasing L_y. We highlight the scalability of our system and its advantage over other schemes [26,54] in two aspects: Fig. 3(b) shows identical physics with scaled-up sizes, and Figs. 3(c)–3(f) manifest our studies with increasing L_y.

We now demonstrate a dynamical control over DSP edge states with $(\xi_x, l_B, \omega_B, \Omega_c, \Delta_p) = (2000, 0.4\text{ mm}, 1.7\times 10^{-3}\Gamma, 1.84\Gamma, 10\Gamma)$. Initially, only Ω_c^R is turned on, and then we pump the system by injecting Ω_p^R of transverse width $w = 0.5$ mm, with the boundary condition $\Omega_p^R(-L_x/2, y) = \exp[-(y/w)^2 - i(\omega_B t - ky)]$ and $k = L_x/(2l_B^2)$ at the left edge. As depicted in Fig. 4(a), ρ_{21} occurs at 0.06 ms in both the edge ($|x| > 0.5$ mm) and the bulk region ($|x| \leqslant 0.5$ mm). Subsequently, Ω_c^L, Ω_c^F, and Ω_c^B are switched on at 0.07 ms to generate a synthetic out-of-plane $\vec{B}_1$. $|\rho_{21}|^2$ subsequently vanishes in the bulk and clockwise propagates along the edge; see Fig. 4(b). We invert $\vec{B}_1$ at 0.27 ms and observe that the DSP edge flow becomes counterclockwise under the in-plane $\vec{B}_1$ in Fig. 4(c). Moreover, the DSP edge state even bypasses the vacuum area (white dashed square) in Fig. 4(d); namely, it is robust and immune to the defect [14–19,21–24,27,29]. We emphasize that in Figs. 4(e)–4(h) we use $(\xi_x, l_B, \omega_B, \Omega_c, \Delta_p) = (400, 0.5\text{ mm}, 8.4\times 10^{-3}\Gamma, 1.84\Gamma, 3.13\Gamma)$, confirming that the above robust chiral edge states can be clearly observed for $\xi_x \geqslant 400$ in our simulations. Figures 4(i)–4(l) illustrate the results of random ξ fluctuating around the average value 400 with maximum 10% variation [Fig. 4(i)]. The density [Figs. 4(j) and 4(l)] and θ [Fig. 4(k)] show that the winding topology is immune to the nonuniformity. Figure 4(m) shows the time sequence of the synthetic field $\vec{B}_1$, which is used for the above results. Figure 4(m) also illustrates the time sequence of another in-plane field, $\vec{B}_2$, which leads to the same results as in Figs. 4(c), 4(d), 4(g), 4(h), and 4(l). Given that the EIT-retrieved light inherits the phase of ρ_{21} [79–81], one can shine a control field along z to retrieve a probe beam carrying topological winding numbers [82–85].

We put forward an EIT-based optical approach to generate synthetic LLs and robust chiral edge states for neutral EIT DSPs in lattice-free media with experimentally realizable parameters. Our system is scalable and provides the capability of dynamical control. Moreover, our scheme can be a versatile quantum simulator [86] for different Hamiltonians and non-Hermitian systems [59,60,87], and it also can generate exotic lights carrying topological phase winding numbers [82–85]. In our system, the scalability and forbidden decay between $n = 1$ and $n = 0$ LL also suggest the application of having many qubits by generating remote DSPs with Rydberg interactions [26]. Analogous to the realization of the Laughlin state of light in Ref. [26], Rydberg EIT [26,52] and a single photon source are viable combinations to introduce strong interaction and engineer a desired filling factor of bosonic quantum Hall state for our scheme.

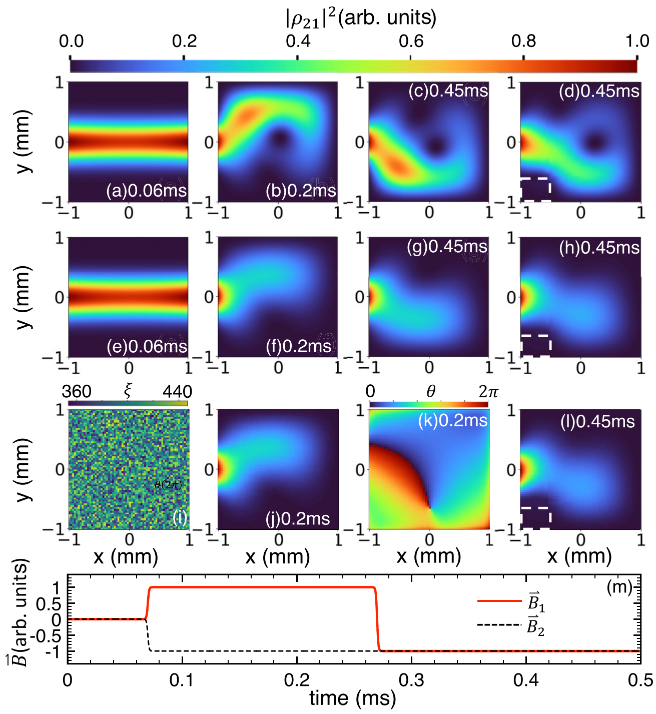

FIG. 4. Dynamical manipulation of initially rightward slow-light DSP entering the medium at $(x, y) = (-1\text{ mm}, 0)$ [(a) and (e)]. Snapshots of the DSP edge state $|\rho_{21}|^2$ with out-of-plane $\vec{B}_1$ at 0.2 ms [(b), (f), and (j)] and in-plane synthetic $\vec{B}_1$ at 0.45 ms [(c), (d), (g), (h), and (l)]. In (d), (h), and (l) the DSP bypasses the vacuum area illustrated by the white dashed square. (j)–(l) Results with fluctuating optical depth $\xi(x, y)$ [shown in (i)] and $l_B = 0.5$ mm, where (k) depicts the θ of (j). (m) The time sequence of the synthetic magnetic field $\vec{B}_1$ (solid red curve) for (a)–(l) where $\vec{B}_1$ is turned on at 0.07 ms and inverted at 0.27 ms. Another in-plane synthetic magnetic field, $\vec{B}_2$ (dashed black curve), also gives identical results to those in (c), (d), (g), and (h). We have uniform $(\xi_x, l_B) = (2000,\ 0.4\text{ mm})$ for (a)–(d) and uniform $(\xi_x, l_B) = (400,\ 0.5\text{ mm})$ for (e)–(h).

We acknowledge insightful discussions with J. Simon, N. Schine, S.-K. Yip, N.-C. Chiu, K.-Y. Lin, and C.-A. Chen. Y.-H.K., S.-Y.L., S.-W.S., and W.-T.L. are supported by the National Science and Technology Council, Taiwan (Grants No. 109-2639-M-007-002-ASP, No. 110-2112-M-008-027-MY3, No. 110-2639-M-007 -001-ASP, No. 111-2923-M-008-004-MY3 & No. 111-2639-M-007-001-ASP). I-K.L. was supported by the Quantera ERA-NET cofund project NAQUAS through the Engineering and Physical Science Research Council, Grant No. EP/R043434/1. G.J. was supported by Project No. S-LLT-22-2 of the Research Council of Lithuania, G.J. and J.R. were also supported by the

National Center for Theoretical Sciences, Taiwan. Y.-J.L. was supported by MOST Grants No. 108-2112-M-001-033-MY3 and No. 111-2112-M-001-048-MY3 and the Thematic Research Program of Academia Sinica. W.-T.L. and Y.-J.L. acknowledge support from Center for Quantum Technology, Hsinchu, Taiwan.

[1] K. v. Klitzing, G. Dorda, and M. Pepper, New method for high-accuracy determination of the fine-structure constant based on quantized Hall resistance, Phys. Rev. Lett. **45**, 494 (1980).
[2] R. B. Laughlin, Quantized Hall conductivity in two dimensions, Phys. Rev. B **23**, 5632 (1981).
[3] D. J. Thouless, M. Kohmoto, M. P. Nightingale, and M. den Nijs, Quantized Hall conductance in a two-dimensional periodic potential, Phys. Rev. Lett. **49**, 405 (1982).
[4] K. von Klitzing, Quantum Hall effect: Discovery and application, Annu. Rev. Condens. Matter Phys. **8**, 13 (2017).
[5] T. H. Hansson, M. Hermanns, S. H. Simon, and S. F. Viefers, Quantum Hall physics: Hierarchies and conformal field theory techniques, Rev. Mod. Phys. **89**, 025005 (2017).
[6] K. von Klitzing, T. Chakraborty, P. Kim, V. Madhavan, X. Dai, J. McIver, Y. Tokura, L. Savary, D. Smirnova, A. M. Rey, C. Felser, J. Gooth, and X. Qi, 40 years of the quantum Hall effect, Nat. Rev. Phys. **2**, 397 (2020).
[7] J. Dalibard, F. Gerbier, G. Juzeliūnas, and P. Öhberg, Colloquium: Artificial gauge potentials for neutral atoms, Rev. Mod. Phys. **83**, 1523 (2011).
[8] M. Lewenstein, S. Anna, and A. Verònica, *Ultracold Atoms in Optical Lattices: Simulating Quantum Many-Body Systems* (Oxford University Press, Oxford, 2012).
[9] N. Goldman, G. Juzeliūnas, P. Öhberg, and I. B. Spielman, Light-induced gauge fields for ultracold atoms, Rep. Prog. Phys. **77**, 126401 (2014).
[10] N. Goldman, J. C. Budich, and P. Zoller, Topological quantum matter with ultracold gases in optical lattices, Nat. Phys. **12**, 639 (2016).
[11] Y.-J. Lin and I. B. Spielman, Synthetic gauge potentials for ultracold neutral atoms, J. Phys. B: At. Mol. Opt. Phys. **49**, 183001 (2016).
[12] N. R. Cooper, J. Dalibard, and I. B. Spielman, Topological bands for ultracold atoms, Rev. Mod. Phys. **91**, 015005 (2019).
[13] V. Galitski, I. B. Spielman, and G. Juzeliūnas, Artificial gauge fields with ultracold atoms, Phys. Today **72**(1), 38 (2019).
[14] M. Hafezi, A. S. Sørensen, E. Demler, and M. D. Lukin, Fractional quantum Hall effect in optical lattices, Phys. Rev. A **76**, 023613 (2007).
[15] F. D. M. Haldane and S. Raghu, Possible realization of directional optical waveguides in photonic crystals with broken time-reversal symmetry, Phys. Rev. Lett. **100**, 013904 (2008).
[16] M. Hafezi, S. Mittal, J. Fan, A. Migdall, and J. M. Taylor, Imaging topological edge states in silicon photonics, Nat. Photon. **7**, 1001 (2013).
[17] M. C. Rechtsman, J. M. Zeuner, Y. Plotnik, Y. Lumer, D. Podolsky, F. Dreisow, S. Nolte, M. Segev, and A. Szameit, Photonic Floquet topological insulators, Nature (London) **496**, 196 (2013).
[18] D.-W. Wang, H. Cai, L. Yuan, S.-Y. Zhu, and R.-B. Liu, Topological phase transitions in superradiance lattices, Optica **2**, 712 (2015).
[19] M. Schmidt, S. Kessler, V. Peano, O. Painter, and F. Marquardt, Optomechanical creation of magnetic fields for photons on a lattice, Optica **2**, 635 (2015).
[20] N. Schine, A. Ryou, A. Gromov, A. Sommer, and J. Simon, Synthetic Landau levels for photons, Nature (London) **534**, 671 (2016).
[21] M. Minkov and V. Savona, Haldane quantum Hall effect for light in a dynamically modulated array of resonators, Optica **3**, 200 (2016).
[22] P. St-Jean, V. Goblot, E. Galopin, A. Lemaître, T. Ozawa, L. Le Gratiet, I. Sagnes, J. Bloch, and A. Amo, Lasing in topological edge states of a one-dimensional lattice, Nat. Photon. **11**, 651 (2017).
[23] M. A. Bandres, S. Wittek, G. Harari, M. Parto, J. Ren, M. Segev, D. N. Christodoulides, and M. Khajavikhan, Topological insulator laser: Experiments, Science **359**, eaar4005 (2018).
[24] S. Mukherjee, H. K. Chandrasekharan, P. Öhberg, N. Goldman, and R. R. Thomson, State-recycling and time-resolved imaging in topological photonic lattices, Nat. Commun. **9**, 4209 (2018).
[25] T. Ozawa, H. M. Price, A. Amo, N. Goldman, M. Hafezi, L. Lu, M. C. Rechtsman, D. Schuster, J. Simon, O. Zilberberg, and I. Carusotto, Topological photonics, Rev. Mod. Phys. **91**, 015006 (2019).
[26] L. W. Clark, N. Schine, C. Baum, N. Jia, and J. Simon, Observation of Laughlin states made of light, Nature (London) **582**, 41 (2020).
[27] A. D'Errico, F. Cardano, M. Maffei, A. Dauphin, R. Barboza, C. Esposito, B. Piccirillo, M. Lewenstein, P. Massignan, and L. Marrucci, Two-dimensional topological quantum walks in the momentum space of structured light, Optica **7**, 108 (2020).
[28] I. Carusotto, A. A. Houck, A. J. Kollár, P. Roushan, D. I. Schuster, and J. Simon, Photonic materials in circuit quantum electrodynamics, Nat. Phys. **16**, 268 (2020).
[29] O. Jamadi, E. Rozas, G. Salerno, M. Milićević, T. Ozawa, I. Sagnes, A. Lemaître, L. Le Gratiet, A. Harouri, I. Carusotto, J. Bloch, and A. Amo, Direct observation of photonic Landau levels and helical edge states in strained honeycomb lattices, Light Sci. Appl. **9**, 144 (2020).
[30] O. Kocharovskaya and Y. I. Khanin, Population trapping and coherent bleaching of a three-level medium by a periodic train of ultrashort pulses, Zh. Eksp. Teor. Fiz. **90**, 1610 (1986).
[31] E. Arimondo, Coherent population trapping in laser spectroscopy, Prog. Opt. **35**, 257 (1996).
[32] S. E. Harris, Electromagnetically induced transparency, Phys. Today **50**(7), 36 (1997).
[33] M. D. Lukin, Colloquium: Trapping and manipulating photon states in atomic ensembles, Rev. Mod. Phys. **75**, 457 (2003).
[34] M. Fleischhauer, A. Imamoglu, and J. P. Marangos, Electromagnetically induced transparency: Optics in coherent media, Rev. Mod. Phys. **77**, 633 (2005).
[35] N. V. Vitanov, A. A. Rangelov, B. W. Shore, and K. Bergmann, Stimulated Raman adiabatic passage in physics, chemistry, and beyond, Rev. Mod. Phys. **89**, 015006 (2017).
[36] K.-J. Boller, A. Imamoğlu, and S. E. Harris, Observation of electromagnetically induced transparency, Phys. Rev. Lett. **66**, 2593 (1991).

[37] L. V. Hau, S. E. Harris, Z. Dutton, and C. H. Behroozi, Light speed reduction to 17 metres per second in an ultracold atomic gas, Nature (London) **397**, 594 (1999).

[38] M. Fleischhauer and M. D. Lukin, Dark-state polaritons in electromagnetically induced transparency, Phys. Rev. Lett. **84**, 5094 (2000).

[39] G. Juzeliūnas and H. J. Carmichael, Systematic formulation of slow polaritons in atomic gases, Phys. Rev. A **65**, 021601(R) (2002).

[40] A. S. Zibrov, A. B. Matsko, O. Kocharovskaya, Y. V. Rostovtsev, G. R. Welch, and M. O. Scully, Transporting and time reversing light via atomic coherence, Phys. Rev. Lett. **88**, 103601 (2002).

[41] M. Bajcsy, A. S. Zibrov, and M. D. Lukin, Stationary pulses of light in an atomic medium, Nature (London) **426**, 638 (2003).

[42] S. A. Moiseev and B. S. Ham, Quantum manipulation of two-color stationary light: Quantum wavelength conversion, Phys. Rev. A **73**, 033812 (2006).

[43] F. E. Zimmer, J. Otterbach, R. G. Unanyan, B. W. Shore, and M. Fleischhauer, Dark-state polaritons for multicomponent and stationary light fields, Phys. Rev. A **77**, 063823 (2008).

[44] Y.-W. Lin, W.-T. Liao, T. Peters, H.-C. Chou, J.-S. Wang, H.-W. Cho, P.-C. Kuan, and I. A. Yu, Stationary light pulses in cold atomic media and without Bragg gratings, Phys. Rev. Lett. **102**, 213601 (2009).

[45] A. V. Gorshkov, J. Otterbach, M. Fleischhauer, T. Pohl, and M. D. Lukin, Photon-photon interactions via Rydberg blockade, Phys. Rev. Lett. **107**, 133602 (2011).

[46] D. Petrosyan, J. Otterbach, and M. Fleischhauer, Electromagnetically induced transparency with Rydberg atoms, Phys. Rev. Lett. **107**, 213601 (2011).

[47] T. Peyronel, O. Firstenberg, Q.-Y. Liang, S. Hofferberth, A. V. Gorshkov, T. Pohl, M. D. Lukin, and V. Vuletić, Quantum nonlinear optics with single photons enabled by strongly interacting atoms, Nature (London) **488**, 57 (2012).

[48] J. D. Pritchard, K. J. Weatherill, and C. S. Adams, Nonlinear optics using cold Rydberg atoms, in *Annual Review of Cold Atoms and Molecules* Vol. 1 (World Scientific, Singapore, 2012), pp. 301–350.

[49] M. Gärttner, S. Whitlock, D. W. Schönleber, and J. Evers, Collective excitation of Rydberg-atom ensembles beyond the superatom model, Phys. Rev. Lett. **113**, 233002 (2014).

[50] C. R. Murray and T. Pohl, Coherent photon manipulation in interacting atomic ensembles, Phys. Rev. X **7**, 031007 (2017).

[51] D. Roy, C. M. Wilson, and O. Firstenberg, Colloquium: Strongly interacting photons in one-dimensional continuum, Rev. Mod. Phys. **89**, 021001 (2017).

[52] K.-T. Chen, B. Kim, C.-C. Su, S.-S. Hsiao, S.-J. Huang, W.-T. Liao, and I. A. Yu, Increasing the decoherence rate of Rydberg polaritons due to accumulating dark Rydberg atoms, Phys. Rev. Res. **4**, 023024 (2022).

[53] D. C. Tsui, H. L. Stormer, and A. C. Gossard, Two-dimensional magnetotransport in the extreme quantum limit, Phys. Rev. Lett. **48**, 1559 (1982).

[54] J. Otterbach, J. Ruseckas, R. G. Unanyan, G. Juzeliūnas, and M. Fleischhauer, Effective magnetic fields for stationary light, Phys. Rev. Lett. **104**, 033903 (2010).

[55] N. R. Cooper, Rapidly rotating atomic gases, Adv. Phys. **57**, 539 (2008).

[56] P. C. Haljan, I. Coddington, P. Engels, and E. A. Cornell, Driving Bose-Einstein-condensate vorticity with a rotating normal cloud, Phys. Rev. Lett. **87**, 210403 (2001).

[57] A. Di Piazza, C. Müller, K. Z. Hatsagortsyan, and C. H. Keitel, Extremely high-intensity laser interactions with fundamental quantum systems, Rev. Mod. Phys. **84**, 1177 (2012).

[58] M. A. Khamehchi, K. Hossain, M. E. Mossman, Y. Zhang, T. Busch, M. M. Forbes, and P. Engels, Negative-mass hydrodynamics in a spin-orbit–coupled Bose-Einstein condensate, Phys. Rev. Lett. **118**, 155301 (2017).

[59] C. M. Bender and S. Boettcher, Real spectra in non-Hermitian Hamiltonians having $\mathcal{PT}$ symmetry, Phys. Rev. Lett. **80**, 5243 (1998).

[60] C. E. Rüter, K. G Makris, R. El-Ganainy, D. N. Christodoulides, M. Segev, and D. Kip, Observation of parity–time symmetry in optics, Nat. Phys. **6**, 192 (2010).

[61] G. T. Campbell, Y.-W. Cho, J. Su, J. Everett, N. Robins, P. K. Lam, and B. Buchler, Direct imaging of slow, stored and stationary EIT polaritons, Quantum Sci. Technol. **2**, 034010 (2017).

[62] S.-W. Su, Z.-K. Lu, S.-C. Gou, and W.-T. Liao, Controllable vacuum-induced diffraction of matter-wave superradiance using an all-optical dispersive cavity, Sci. Rep. **6**, 35402 (2016).

[63] Y.-H. Kuan and W.-T. Liao, Transition between amplified spontaneous emission and superfluorescence in a longitudinally pumped medium by an x-ray free-electron-laser pulse, Phys. Rev. A **101**, 023836 (2020).

[64] M. Z. Hasan and C. L. Kane, Colloquium: Topological insulators, Rev. Mod. Phys. **82**, 3045 (2010).

[65] D. Xiao, M.-C. Chang, and Q. Niu, Berry phase effects on electronic properties, Rev. Mod. Phys. **82**, 1959 (2010).

[66] Y.-J. Lin, R. L. Compton, K. Jiménez-García, J. V. Porto, and I. B. Spielman, Synthetic magnetic fields for ultracold neutral atoms, Nature (London) **462**, 628 (2009).

[67] Y.-J. Lin, R. L. Compton, K. Jimenez-Garcia, W. D. Phillips, J. V. Porto, and I. B. Spielman, A synthetic electric force acting on neutral atoms, Nat. Phys. **7**, 531 (2011).

[68] Y.-F. Hsiao, H.-S. Chen, P.-J. Tsai, and Y.-C. Chen, Cold atomic media with ultrahigh optical depths, Phys. Rev. A **90**, 055401 (2014).

[69] F. Blatt, T. Halfmann, and T. Peters, One-dimensional ultracold medium of extreme optical depth, Opt. Lett. **39**, 446 (2014).

[70] Y.-F. Hsiao, P.-J. Tsai, H.-S. Chen, S.-X. Lin, C.-C. Hung, C.-H. Lee, Y.-H. Chen, Y.-F. Chen, I. A. Yu, and Y.-C. Chen, Highly efficient coherent optical memory based on electromagnetically induced transparency, Phys. Rev. Lett. **120**, 183602 (2018).

[71] A. L. Gaunt, T. F. Schmidutz, I. Gotlibovych, R. P. Smith, and Z. Hadzibabic, Bose-Einstein condensation of atoms in a uniform potential, Phys. Rev. Lett. **110**, 200406 (2013).

[72] N. Navon, R. P. Smith, and Z. Hadzibabic, Quantum gases in optical boxes, Nat. Phys. **17**, 1334 (2021).

[73] Here we provide the calculations for the 2D atomic gas with ξ up to $\sim$2000, which are based on experimental data from Ref. [88]. Evaporative cooling reduces the atom number N and increases the density, and we obtain the scaling law in Ref. [88]: temperature $T \propto N^{0.89}$ and $n_{3D} \propto N^{-1.36}$. For example, the numbers for Fig. 3 with $\xi_x = 2000$, $L_x = 2$ or 4 mm, and $L_y = 2$ mm are as follows: We start with a nonuniform 3D cloud with $N = 1.3 \times 10^{10}$ atoms and

$n_{3D} = 2.7 \times 10^{11}$ cm^{-3} and then increase n_{3D} to 2.7×10^{12} cm^{-3} with a reduced number $N = 2.2 \times 10^9$. The volume is about 0.8 mm^3, where we make $(L_x, L_y, L_z) = (2, 2, 0.2)$ mm. To make $L_x = 4$ mm with a fixed $\xi_x = 2000$, we use a smaller density $n_{3D} = 1.35 \times 10^{12}$ cm^{-3} and a larger number $N = 3.7 \times 10^9$ with $(L_x, L_y, L_z) = (4, 2, 0.3)$ mm.

[74] V. Gavryusev, A. Signoles, M. Ferreira-Cao, G. Zürn, C. S. Hofmann, G. Günter, H. Schempp, M. Robert-de Saint-Vincent, S. Whitlock, and M. Weidemüller, Density matrix reconstruction of three-level atoms via Rydberg electromagnetically induced transparency, J. Phys. B: At. Mol. Opt. Phys. **49**, 164002 (2016).

[75] O. Kocharovskaya, Y. Rostovtsev, and M. O. Scully, Stopping light via hot atoms, Phys. Rev. Lett. **86**, 628 (2001).

[76] D. F. Phillips, A. Fleischhauer, A. Mair, R. L. Walsworth, and M. D. Lukin, Storage of light in atomic vapor, Phys. Rev. Lett. **86**, 783 (2001).

[77] Y.-H. Chen, M.-J. Lee, I.-C. Wang, S. Du, Y.-F. Chen, Y.-C. Chen, and I. A. Yu, Coherent optical memory with high storage efficiency and large fractional delay, Phys. Rev. Lett. **110**, 083601 (2013).

[78] J. Radić, T. A. Sedrakyan, I. B. Spielman, and V. Galitski, Vortices in spin-orbit-coupled Bose-Einstein condensates, Phys. Rev. A **84**, 063604 (2011).

[79] Y.-F. Chen, C.-Y. Wang, S.-H. Wang, and I. A. Yu, Low-light-level cross-phase-modulation based on stored light pulses, Phys. Rev. Lett. **96**, 043603 (2006).

[80] W.-T. Liao, C. H. Keitel, and A. Pálffy, All-electromagnetic control of broadband quantum excitations using gradient photon echoes, Phys. Rev. Lett. **113**, 123602 (2014).

[81] S.-W. Su, S.-C. Gou, L. Y. Chew, Y.-Y. Chang, I. A. Yu, A. Kalachev, and W.-T. Liao, Setting a disordered password on a photonic memory, Phys. Rev. A **95**, 061805(R) (2017).

[82] N. R. Heckenberg, R. McDuff, C. P. Smith, and A. G. White, Generation of optical phase singularities by computer-generated holograms, Opt. Lett. **17**, 221 (1992).

[83] L. Marrucci, C. Manzo, and D. Paparo, Optical spin-to-orbital angular momentum conversion in inhomogeneous anisotropic media, Phys. Rev. Lett. **96**, 163905 (2006).

[84] P. Vaity, J. Banerji, and R. P. Singh, Measuring the topological charge of an optical vortex by using a tilted convex lens, Phys. Lett. A **377**, 1154 (2013).

[85] D. Naidoo, F. S. Roux, A. Dudley, I. Litvin, B. Piccirillo, L. Marrucci, and A. Forbes, Controlled generation of higher-order Poincaré sphere beams from a laser, Nat. Photon. **10**, 327 (2016).

[86] I. M. Georgescu, S. Ashhab, and F. Nori, Quantum simulation, Rev. Mod. Phys. **86**, 153 (2014).

[87] Y. Ashida, Z. Gong, and M. Ueda, Non-Hermitian physics, Adv. Phys. **69**, 249 (2020).

[88] Y.-J. Lin, A. R. Perry, R. L. Compton, I. B. Spielman, and J. V. Porto, Rapid production of ^{87}Rb Bose-Einstein condensates in a combined magnetic and optical potential, Phys. Rev. A **79**, 063631 (2009).